0026-895X/10/7702-255–261$20.00
MOLECULAR PHARMACOLOGY
Copyright © 2010 The American Society for Pharmacology and Experimental Therapeutics
Mol Pharmacol 77:255–261, 2010

Vol. 77, No. 2
60327/3552761
Printed in U.S.A.

A Novel Roscovitine Derivative Potently Induces G_1-Phase Arrest in Platelet-Derived Growth Factor-BB-Activated Vascular Smooth Muscle Cells[S]

Irene M. Sroka, Elke H. Heiss, Libor Havlicek, Frank Totzke, Yasmin Aristei, Paul Pechan, Michael H. G. Kubbutat, Miroslav Strnad, and Verena M. Dirsch

Department of Pharmacognosy, University of Vienna, Vienna, Austria (I.M.S., E.H.H., V.M.D.); Laboratory of Growth Regulators, Palacký University and Institute of Experimental Botany ASCR, Olomouc, Czech Republic (L.H., M.S.); ProQinase GmbH, Freiburg, Germany (F.T., M.H.G.K.); C3 BIO GmbH, Munich, Germany (P.P.); and Department of Chemistry, Laboratory for Chemometrics and Chemoinformatics, University of Perugia, Perugia, Italy (Y.A.)

Received August 14, 2009; accepted November 2, 2009

ABSTRACT

Abnormal vascular smooth muscle cell (VSMC) proliferation contributes to the pathogenesis of restenosis. Thus, drugs interfering with cell cycle progression in VSMC are promising candidates for an antirestenotic therapy. In this study, we pharmacologically characterize *N*-5-(2-aminocyclohexyl)-*N*-7-benzyl-3-isopropyl-1(2)H-pyrazolo[4,3-*d*]pyrimidine-5,7-di-amine (LGR1406), a novel derivative of the cyclin-dependent kinase (CDK) inhibitor roscovitine (ROSC), in PDGF-BB-activated VSMC. Cell proliferation was quantified measuring DNA synthesis via 5-bromo-2′-deoxyuridine incorporation. Analysis of cell cycle distribution was done by flow cytometry using propidium iodide-stained nuclei. Key regulators of the cell cycle and relevant signaling pathways were dissected by Western blot analyses. In addition, in vitro kinase assays and in silico studies regarding the pharmacokinetic profile of both compounds were performed. LGR1406 shows a stronger (IC_{50} = 3.0 μM) antiproliferative activity than ROSC (IC_{50} = 16.9 μM), halting VSMCs in G_0/G_1 phase of the cell cycle, whereas ROSC does not arrest but rather delays cell cycle progression. Neither of the compounds interferes with early PDGF-BB-induced signaling pathways (p38, extracellular signal-regulated kinase 1/2, c-Jun NH_2-terminal kinase, Akt, signal transducer and activator of transcription 3), and both inhibit CDKs, with LGR1406 exerting a slightly higher potency against CDK1/2 and 4 than ROSC. Expression of cyclins A and E as well as hyperphosphorylation of the pocket proteins retinoblastoma protein and p107 are negatively affected by both compounds, although to a different extent. In silico calculations predicted a much higher metabolic stability for LGR1406 compared with ROSC. Altogether, ROSC derivatives, such as LGR1406 seem to be promising compounds for further development in antirestenotic therapy.

Developing strategies against restenosis, the renarrowing of an artery after angioplastic interventions, remains an important goal of vascular biology and pharmacological research. Currently, drug-eluting stents have become the treatment of choice for patients undergoing percutaneous coronary revascularization (Kukreja et al., 2008). Current marketed first-generation drug eluting stents use drugs such as rapamycin and paclitaxel targeting mammalian target of rapamycin and tubulin, respectively (Windecker and Jüni, 2008). Unfortunately, some concerns have been raised recently due to a potential increased risk of late-stent thrombosis (Steffel et al., 2008). Therefore, the identification of new drug candidates interfering with vascular smooth muscle cell (VSMC) proliferation using mechanisms other than rapamycin and paclitaxel is an important pharmacological topic.

Roscovitine (ROSC) has been characterized as a selective inhibitor of cyclin dependent kinases (CDK) 1, 2, and 5 in enzyme-based assays (Meijer et al., 1997), inhibiting the proliferation of various cell types ranging from numerous cancer cell lines to keratinocytes and fibroblasts. The ob-

This work was supported by the European Union within the sixth framework program project "ProKinase Research" [Grant LSHB-CT-2004-503467]; the Czech Grant Agency [Grant 8301/08/1649]; and the Czech Ministry of Education [Grant MSM 6198959216].

Article, publication date, and citation information can be found at http://molpharm.aspetjournals.org.

doi:10.1124/mol.109.060327.

[S] The online version of this article (available at http://molpharm.aspetjournals.org) contains supplemental material.

ABBREVIATIONS: VSMC, vascular smooth muscle cell; Ang II, angiotensin II; BrdU, 5-bromo-2′-deoxyuridine; CDK, cyclin-dependent kinase; DMSO, dimethyl sulfoxide; ERK, extracellular signal-regulated kinase; HSA, human serum albumin; ISS, in-stent stenosis; MAPK, mitogen-activated protein kinase; PBS, phosphate-buffered saline; PDGF, platelet-derived growth factor; Rb, retinoblastoma protein; ROSC, roscovitine; LGR1406, *N*-5-(2-aminocyclohexyl)-*N*-7-benzyl-3-isopropyl-1(2)H-pyrazolo[4,3-*d*]pyrimidine-5,7-di-amine; PI, propidium iodide; VD, volume distribution; ANOVA, analysis of variance.

served effects, however, seem to be strongly dependent on cell type, stimuli, and treatment conditions (Alessi et al., 1998; Mgbonyebi et al., 1999; Meijer and Raymond, 2003; Atanasova et al., 2005). Currently ROSC is undergoing phase II clinical trials as an anticancer drug (Benson et al., 2007). However, publications regarding ROSC and cell types involved in other proliferative disorders, such as VSMC, are very limited.

Although ROSC shows selectivity for CDKs compared with other kinases (Bach et al., 2005), effort is made to optimize ROSC to obtain compounds exerting higher specificity and higher potency (Bettayeb et al., 2008; Oumata et al., 2008). The IC_{50} of ROSC for growth inhibition is approximately 25 μM depending on cell type.

Thus, the aim of this study was to select out of a panel of synthesized ROSC derivatives the most effective candidate in terms of its potency to inhibit PDGF-induced VSMC proliferation and to characterize its mode of action in comparison with ROSC itself, which was not thoroughly characterized in VSMCs before. As a model, we used PDGF-BB-activated VSMCs, because PDGF-BB is the major proliferative stimulus for VSMC (Heldin and Westermark, 1990).

We show here that the ROSC derivative LGR1406 is a more potent inhibitor of PDGF-induced VSMC proliferation than ROSC and that ROSC treatment only delays the progress of the cell cycle, whereas LGR1406 potently arrests VSMCs in G_1 phase. Moreover, in silico data predict a higher metabolic stability of LGR1406 compared with ROSC.

Materials and Methods

Chemicals and Reagents. Unless noted otherwise, all cell culture reagents and media were obtained from Lonza Group Ltd. (Basel, Switzerland), and all other reagents were from Carl Roth (Karlsruhe, Germany). Trypsin, collagenase II, and Ham's F-12 medium were purchased from Invitrogen (Carlsbad, CA), and DMSO was from Fluka (Buchs, Switzerland). Roscovitine was obtained from Calbiochem (San Diego, CA), and recombinant human PDGF-BB was from Bachem (Weil am Rhein, Germany). Anti-cyclin E, anti-cyclin A, anti-α-tubulin, and anti-p107 antibodies were purchased from Santa Cruz Biotechnology (Santa Cruz, CA), anti-phospho-Ser807+811 retinoblastoma protein, anti-cyclin D1, and rabbit IgG antibodies were from New England Biolabs (Ipswich, MA). The mouse IgG antibody was obtained from Upstate (Billerica, MA). The fluorescein isothiocyanate-labeled anti-smooth muscle-α-actin antibody and luminol were purchased from Sigma-Aldrich (St. Louis, MO). Complete protease inhibitor was obtained from Roche Diagnostics (Basel, Switzerland). Immunoblot polyvinylidene difluoride membrane and Precision Plus Protein standard were purchased from Bio-Rad (Hercules, CA).

LGR1406 synthesis. LGR1406 was prepared by synthetic approach described by Krystof et al. (2006). The product was purified by column chromatography as amorphous solid glass residue, with a melting point of 95 to 105°C. mass spectrometry electrospray ionization$^+$: $[M+H]^+$ = 380,3 (100). ^{1}H NMR (300 MHz, DMSO-d^6): 1.01 to 1.31 m (3H, 24a, 24b, 25a), 1.32 d (6H, J = 7,0 Hz, 19), 1.44 to 1.68 m (3H, 23a, 23b, 26a), 1.84 bd (1H, 25b), 2.01 bd (1H, 26b), 2.54 m (1H, 22), 3.16 sept (1H, *J* = 7.0 Hz, 18), 3.43 m (1H, 21), 4.68 s (2H, 11), 5.82 d (1H, *J* = 7,7 Hz, 20), 7.25 t (1H, 15), 7.34 t (2H, 14 + 16), 7.39 d (2H, 13 + 17), 7.75 bs (1H, 10), 11.98 bs (1H, 1). ^{13}C NMR (300 MHz, DMSO-d^6): 21.6 (19); 21.7 (19); 24.8 (24); 24.9 (25); 25.8 (18); 31.9 (26); 34.3 (23); 43.0 (11); 54.0 (22); 57.1 (21); 126.8 (15); 127.5 (13 + 17); 128.3 (14 + 16); 136.0; 139.6 (12); 145.7; 150.6 (7); 157.4; 158.1; 168.6. Analysis ($C_{21}H_{29}N_7$) calculated, C = 66.46%; H = 7.70%; N = 25.83%; found, C = 66.70%; H = 7.66%; N = 25.64%.

Vascular Smooth Muscle Cell Isolation and Cultivation. VSMCs employed in this study originate from two independent isolations from rat thoracic aortas of three sibling Sprague-Dawley rats each. Aortas were thoroughly cleaned from surrounding tissue, washed in PBS, and incubated with digestion buffer for 3 h (Ham's F-12 medium supplemented with 253 U/ml collagenase II, 10 mM HEPES, 0.28 mM ascorbic acid, and 0.1% bovine serum albumin) for 15 min at 37°C. After centrifugation for 10 min at 230*g*, the supernatant was discarded, and cells were incubated with standard medium (Dulbecco's modified Eagle's medium supplemented with 2 mM L-glutamine, 100 U/ml penicillin, 100 μg/ml streptomycin, and 10% calf serum) in a humidified incubator at 37°C in the presence of 5% CO_2. Purity of VSMC cultures was checked by immunostaining of α-smooth muscle actin with a fluorescein isothiocyanate-labeled antibody. VSMCs were seeded at the indicated density and after 24 h were serum-starved (standard medium, 0.1% calf serum) for another 24 h before all experiments. Passages 6 to 14 were used.

5-Bromo-2′-deoxyuridine Incorporation Assay. As a measurement of DNA synthesis, 5-bromo-2′-deoxyuridine (BrdU) incorporation was determined using a cell proliferation kit (Roche Diagnostics). VSMCs were seeded into black 96-well plates (2×10^4 cells/well), serum-starved, pretreated with test compounds or vehicle (DMSO 1%) for 30 min, and subsequently stimulated with PDGF-BB (20 ng/ml). After 4 h, BrdU (10 μM) was added, and cells were further cultivated for 20 h. Afterward, cells were fixed and stained with an enzyme-coupled anti-BrdU antibody according to the manufacturer's instructions. Relative light units were determined using a 96-well plate reader (Tecan GENios Pro; Tecan Group Ltd., Männedorf, Switzerland). Experiments were performed in triplicate.

Propidium Iodide Staining and Flow Cytometric Cell Cycle Analysis. Cell cycle distribution of VSMC was determined after propidium iodide (PI) staining according to Riccardi and Nicoletti (2006). In brief, VSMCs were seeded into 12-well plates (1×10^5 cells/well), serum-starved, pretreated with test compounds or vehicle (DMSO 1%) for 30 min, and subsequently stimulated with PDGF-BB (20 ng/ml). After 8 to 28 h, cells were trypsinized, fixed with ice-cold hypotonic fluorochrome solution buffer [0.1% (w/v), sodium citrate 0.1% (v/v), and Triton X-100 in PBS] containing 50 μg/ml PI, and incubated for 2 h at 4°C. Cells (10,000) were analyzed by flow cytometry on a FACSCalibur (BD Biosciences, San Jose, CA). Experiments were done in triplicate.

SDS Gel Electrophoresis and Western Blot Analysis. VSMCs were seeded into 60-mm dishes (1×10^6 cells/dish), serum-starved, pretreated with test drugs or vehicle (DMSO 1%) for 30 min, and subsequently stimulated with PDGF-BB (20 ng/ml). Cells were washed with ice-cold PBS, incubated with lysis buffer (50 mM HEPES, 50 mM NaCl, 50 mM NaF, 10 mM $Na_4P_2O_7 \cdot 10H_2O$, 5 mM EDTA, 1 mM phenylmethylsulfonyl fluoride, Complete, and 1% Triton X-100, pH 7.5) for 10 min at 4°C and centrifuged for 10 min at 16,000*g* at 4°C. Supernatants were mixed with 3× SDS sample buffer and heated to 95°C for 5 min. Protein concentrations were determined using Rotiquant reagent according to the manufacturer's instructions (Carl Roth). Standard gel electrophoresis and blotting techniques were used (Bio-Rad). Primary antibodies were diluted 1:1000, and secondary antibodies were diluted 1:10,000. Bands were analyzed with an enhanced chemiluminescence protocol and visualized with an LAS-3000 luminescent image analyser (Fujifilm, Tokyo, Japan) and AIDA software (raytest GmbH, Straubenhardt, Germany).

In Vitro Kinase Assay. The kinases were expressed as human recombinant glutathione transferase or histidine-tagged fusion proteins in Sf6 insect cells and purified using GSH-agarose columns (Sigma-Aldrich) or Ni-NTA Agarose columns (QIAGEN AG, Hilden, Germany). In vitro kinase assays were done in 96-well flash plates (PerkinElmer Life and Analytical Sciences, Waltham, MA) in 50-μl reaction volumes [60 mM HEPES-NaOH, pH 7.3, 3 mM $MgCl_2$, 3 mM $MnCl_2$, 3 μM natrium orthovanadate, 1.2 mM dithiothreitol, 50 μg/ml polyethylene glycol 20000, 1 μM [γ-^{33}P]ATP ($\sim 6.5 \times 10^5$ cpm/well), and 10% compound solution]. LGR1406 dissolved in 10%

DMSO was added in serial dilutions from 1 nM to 10 mM. For substrates and kinases used, see Supplemental Table 1. The plates were incubated at 30°C for 80 min, and the reaction was stopped with 50 μl of 2% (v/v) H_3PO_4. Plates were aspirated, washed two times with 200 μl of double-distilled H_2O, and incorporation of $^{33}P_i$ was determined with a microplate scintillation counter (Microbeta; PerkinElmer Wallac, Gaithersburg, MD). Assays were done in duplicate and were performed with a Beckman Coulter/Segian robotic system (Beckman Coulter, Fullerton, CA). The residual activities for each concentration and the IC_{50} values were calculated using Quattro Workflow version 2.0.2.2. (Quattro Research GmbH, Munich, Germany).

In Silico Prediction of the Pharmacokinetic Profile of LGR1406 Compared with ROSC. VolSurf (Cruciani et al., 2000) is an established computational procedure to produce 2D molecular descriptors from 3D molecular interaction energy grid maps that is used during drug design, pharmacokinetics profiling, and screening (Mannhold et al., 1999; Cruciani et al., 2000; Cianchetta et al., 2004; Crivori et al., 2004; Berellini et al., 2005). For the comparison of the pharmacokinetic profiles of LGR1406 and ROSC, we used the protein binding, volume distribution (VD), and CYP3A4 metabolic stability model. The protein binding model is a qualitative model containing 500 related but chemically diverse compounds. Data report mainly human serum albumin (HSA) binding values between 10 and 100% obtained with spectroscopic techniques. Because HSA is the principal biological carrier of many drugs, it facilitates their conveyance to the target tissues through the circulatory system. The model can be used to project external compounds in the chemical space represented by the model to rank the protein binding profile of external compounds.

The VD model was obtained from more than 600 compounds collected from the literature. The VD data (reported as liters per kilogram) were converted in −Log[VD] values. Low VD values indicate low distribution into tissues, whereas high VD values indicate high distribution into tissues. The VD is of extreme importance in estimating the loading dose necessary to rapidly achieve a desired plasma concentration. VolSurf+ provides a model to estimate the metabolic stability in human CYP3A4 cDNA-expressed microsomal preparation of a drug incubated at a fixed concentration for 60 min with a fixed concentration of protein as well at 37°C. Compounds with a final concentration equal to or greater than 50% of the corresponding control sample were defined as stable, whereas compounds with final concentrations lower than 50% of the corresponding control were defined as unstable. Molecular Discovery Limited (Perugia, Italy) kindly provided free access to the software VolSurf +.

Statistical Analysis. All statistical analyses were calculated using GraphPad PRISM, version 4.03 (GraphPad Software Inc., San Diego, CA). Data are expressed as the means of at least three independent experiments ± S.D. or S.E.M. One-way or two-way ANOVAs and Student's t tests were used for statistical analysis of the results, as indicated in the figure legends. A P value <0.05 was considered to be statistically significant.

Results

Influence of LGR1406 and ROSC on VSMC Proliferation. A panel of 26 synthetic ROSC derivatives was screened for a general antiproliferative activity in VSMCs using crystal violet staining (data not shown). This assay revealed one derivative, LGR1406, with a significantly higher potency than ROSC itself (structures are shown in Fig. 1). We therefore compared the influence of both compounds on PDGF-BB (20 ng/ml)-induced DNA-synthesis using a BrdU incorporation assay. DNA synthesis was dose-dependently reduced by both compounds, with LGR1406 again exerting a stronger antiproliferative activity on VSMCs (IC_{50} = 3 μM) than ROSC (IC_{50} = 17 μM) (Fig. 2).

To exclude potential cytotoxicity, we monitored changes in cell morphology over time compared with staurosporine as a positive control (Allen et al., 2005). Cells treated with up to 5 μM LGR1406 and 20 μM ROSC, respectively, did not show any signs of apoptosis (Supplemental Fig. 1). In addition, in contrast to staurosporine, the number of LGR1406-treated (3–10 μM) and ROSC-treated (15–25 μM) cells after 48 h did not decrease below control, as shown by crystal violet staining (Supplemental Fig. 2). Consistent with these results, trypan blue staining of LGR1406- (3–10 μM) and ROSC-treated (15–25 μM) cells revealed that similar to vehicle-treated control cells, more than 94% of VSMCs were viable after up to 48 h of treatment (data not shown). For further experiments, we therefore used 5 μM LGR1406 and 20 μM ROSC, a concentration of ROSC that is widely used in other cell types (Meijer et al., 1997; Whittaker et al., 2004; Atanasova et al., 2005).

Influence of LGR1406 and ROSC on Cell Cycle Progression and Early PDGF-BB-Induced Signaling Events in VSMC. We next examined whether LGR1406 and ROSC arrest VSMC in a specific cell cycle phase (Fig. 3 and Supplemental Fig. 3). Figure 3 shows the time-dependent entry of serum-starved VSMCs into S phase of the cell cycle upon PDGF-BB stimulation in the absence or presence of LGR1406 and ROSC (8–28 h). PDGF-BB led to a significantly elevated number of cells in S phase as early as 10 h after the addition of the

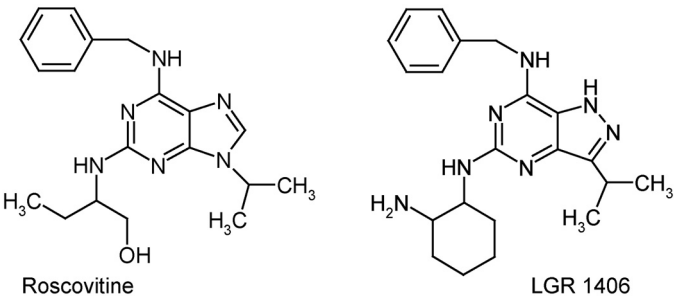

Fig. 1. Chemical structures of ROSC and LGR1406.

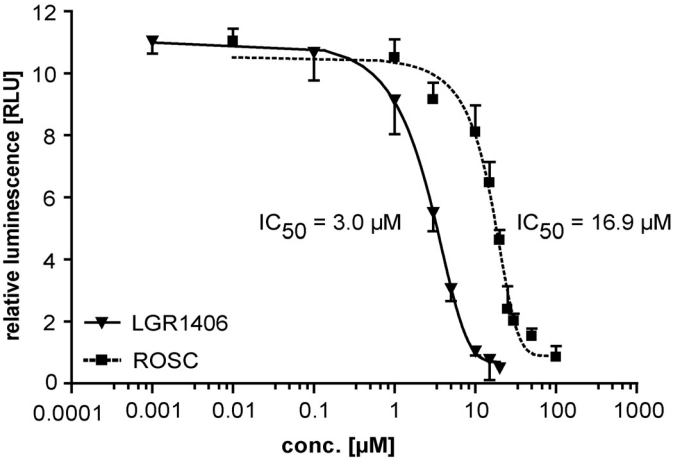

Fig. 2. Dose-response curves obtained for LGR1406 and ROSC measuring DNA synthesis in PDGF-activated VSMC. Serum-starved VSMCs were pretreated with increasing concentrations of LGR1406 (0.1–15 μM) or ROSC (1–100 μM) for 30 min after PDGF (20 ng/ml) treatment. After 4 h, cells were incubated with BrdU and PDGF for an additional 20 h. BrdU incorporation was determined 24 h after cell activation with PDGF-BB. IC_{50} values were calculated by fitting a sigmoidal dose-response curve (variable slope, GraphPad Prism).

stimulus, indicating that the cells pass late G_1 phase after approximately 6 to 8 h and undergo S phase transition after 8 to 10 h (black bars). Treatment with 5 μM LGR1406 completely abrogated the PDGF-BB-induced S-phase entry, whereas 20 μM concentration of the CDK inhibitor ROSC only slightly decreased but delayed cell cycle progression by approximately 8 to 10 h (gray bars). Consistently, ROSC-treated cells also show a delayed entry into G_2/M phase (Supplemental Fig. 3). Further experiments using even up to 25 μM ROSC for up to 48 h showed no accumulation of VSMCs in any phase of the cell cycle (data not shown).

Next we asked whether either of the substances interferes with early signaling events downstream of the PDGF receptor. Using Western blot analyses, we excluded any inhibitory influence of ROSC or LGR1406 on MAPK phosphorylation (p38, ERK, c-Jun N-terminal protein kinase) or the activation of Akt and signal transducer and activator of transcription 3 (Supplemental Fig. 4). Although previous reports implicated an interference of ROSC with MAPK activation (Bach et al., 2005; Li et al., 2008), our results were further corroborated even when using higher concentrations of both compounds (10 μM LGR1406 and 25 μM ROSC) and prolonged time of preincubation (15 h) (data not shown).

Effect of LGR1406 and ROSC on Key Regulators of the Cell Cycle. To further characterize the observed antiproliferative effect on the molecular level, we studied the time-dependent changes in expression and activity of key regulators of the cell cycle upon PDGF-BB stimulation in the presence of LGR1406 and ROSC. Figure 4a shows that cyclin D1 levels are increased from 4 to 24 h after PDGF-BB stimulation. ROSC and LGR1406 did not reduce but even markedly increased cyclin D1 levels compared with control cells, confirming that both compounds did not interfere with early upstream signaling events leading to cell cycle entry and progression. In agreement with the flow cytometric data on S phase entry (Fig. 3), LGR1406 inhibited the expression of the S phase cyclin A, whereas ROSC only delayed the expression of this cyclin (Fig. 4b). In PDGF-activated cells, consistent with the activation of CDK4/6 by cyclin D1 and CDK2 by cyclin A/E (Fig. 4, b and c), the pocket proteins retinoblastoma protein (Rb) and p107, main CDK targets, are hyperphosphorylated from late G_1 phase (6–8 h) onward (Fig. 5). LGR1406 treatment completely abolished whereas ROSC again only delayed the onset of PDGF-BB-induced pocket protein hyperphosphorylation (Fig. 5).

Both compounds inhibited cyclin E expression (Fig. 4c), regulated mainly by the E2F transcription factor family downstream of Rb; however, these data were less clear because the vehicle-treated cells already displayed a high level of cyclin E that was only slightly increased in response to PDGF-BB.

Altogether, the analyses of cyclins and pocket protein phosphorylation suggest that LGR1406 and ROSC indeed directly interfere with CDK activity in PDGF-activated VSMCs. Complete inhibition of pocket protein phosphorylation by LGR1406 points to CDK4/6 as a likely target. We therefore finally performed in vitro CDK assays. A panel of kinases was analyzed using the standardized ProQinase screening platform (ProQinase, Freiburg, Germany). Table 1 shows that LGR1406 had overall lower IC_{50} values against depicted CDKs compared with ROSC, except for CDK6 and CDK7. The overall specificity of LGR1406 was comparable with that of ROSC. The most obvious differences in the in vitro activity profile of both compounds were a high activity of LGR1406 against Aurora A kinase (IC_{50} = 0.6 μM) that was not inhibited by ROSC and a high activity of ROSC against CDK7 (IC_{50} = 1.7 μM) that was not inhibited by LGR1406.

In Silico Prediction of Pharmacokinetic Parameters of LGR1406 and ROSC. To get an idea of whether LGR1406 and ROSC differ in basic pharmacokinetic parameters, we

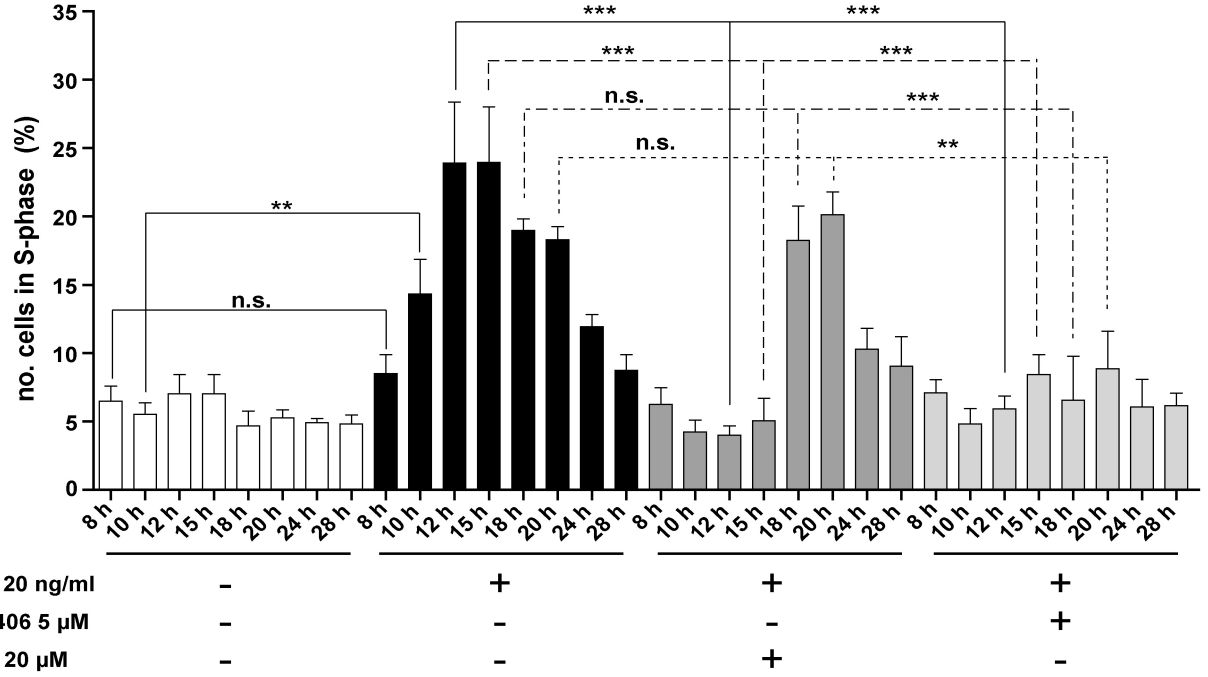

Fig. 3. Influence of LGR1406 and ROSC on PDGF-induced S-phase entry of VSMCs. Serum-starved VSMCs were pretreated for 30 min with LGR1406 (5 μM), ROSC (20 μM), or vehicle (DMSO 1%) and cultured in the presence or absence of PDGF (20 ng/ml). After the indicated periods of time, the percentage of cells in S phase was determined by flow cytometric analysis of PI-stained nuclei. Columns show the mean of three independent experiments ± S.E.M. n.s., not significant; **, $P < 0.01$, ***, $P < 0.001$ (two-way ANOVA followed by Bonferroni post test versus PDGF treatment).

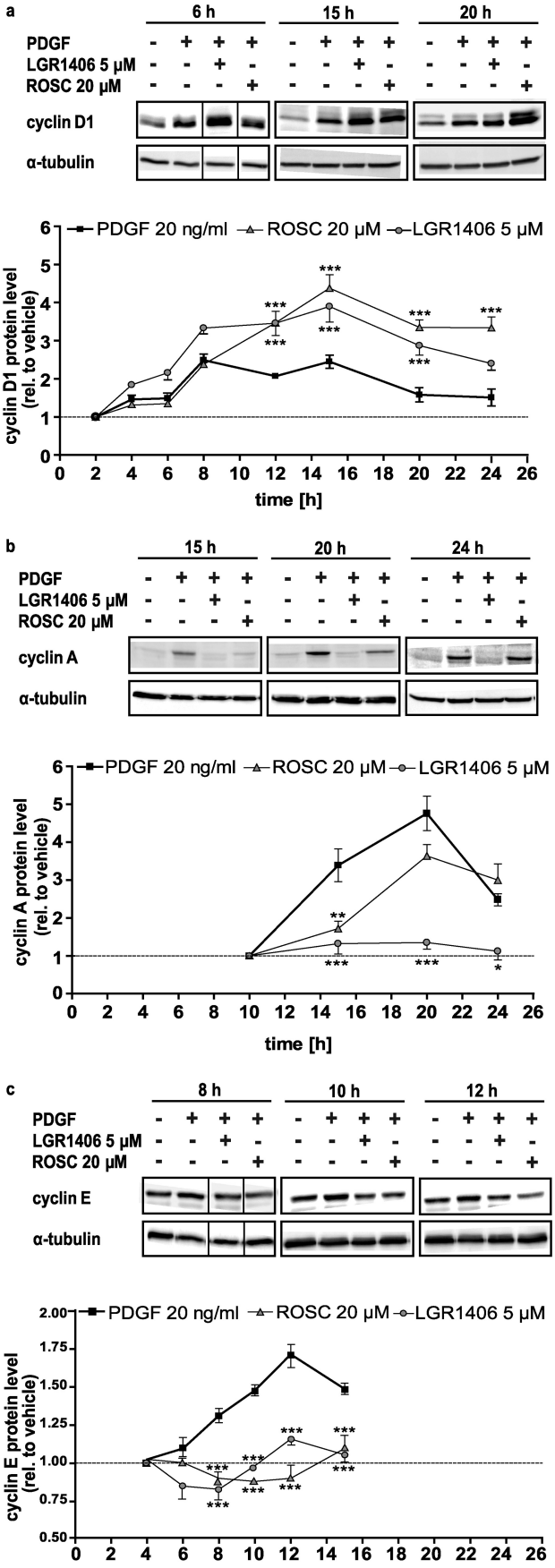

Fig. 4. Influence of LGR1406 and ROSC on cyclin levels. Serum-starved VSMCs were pretreated for 30 min with LGR1406 (5 μM), ROSC (20 μM), or vehicle (DMSO 1%) before stimulation with PDGF-BB (20 ng/ml) for the indicated periods of time. Total cell lysates were then subjected to Western blot analysis for cyclins D1, A, and E, and α-tubulin. Representative Western blots out of at least three independent experiments with consistent results are shown for cyclin D1 (a), cyclin A (b), and cyclin E (c). Graphs depict compiled data of densitometrically evaluated cyclin/tubulin ratios for each time point normalized to the respective unstimulated vehicle control. Shown are means ± S.E.M. *, $P < 0.05$, **, $p < 0.01$, ***, $p < 0.001$ (two-way ANOVA followed by Bonferroni post test versus PDGF treatment).

ran in silico calculations using VolSurf+ software, which predicts certain pharmacokinetic parameters based on comparison with profiles of a collection of >500 related but chemically diverse entities (Crivori et al., 2000). For LGR1406, the software predicted a considerable amount of free drug in the plasma due to 72% binding of LGR1406 to HSA. In a volume distribution model, LGR1406 scored 0.41, which means high achievable concentrations in tissues. In the metabolic stability model, LGR1406 obtained a value of 0.75. This suggests that LGR1406 would show a high fraction of unmetabolized compound after 60 min of incubation at 37°C with CYP3A4-enriched microsomal proteins. We performed the same calculations for ROSC, which yielded comparable values except for the metabolic stability. The calculations resulted in 70% serum binding, a score of 0.49 in the tissue distribution model but substantially lower resistance to CYP3A4 metabolism. In fact, in the metabolic stability model, ROSC obtained a value of 0.47. This means that ROSC would show a fundamentally lower fraction of unmetabolized compound by CYP3A4 compared with LGR1406, suggesting that LGR1406 might have the more suitable pharmacokinetic profile for drug development.

Discussion

Here we show for the first time the antiproliferative activity of ROSC and its derivative LGR1406 in PDGF-BB-activated VSMCs. LGR1406 showed a higher potency regarding the inhibition of DNA synthesis with an apparent IC_{50} of 3.0 μM compared with ROSC with an IC_{50} of 17 μM. A detailed molecular analysis showed that both compounds affect the entry of cells into S phase of the cell cycle, expression of cyclins A and E, and phosphorylation of pocket proteins presumably by the inhibition of CDK activity. However, whereas ROSC only delays these events at 20 μM, LGR1406 elicits complete inhibition at 5 μM.

Although ROSC has been studied extensively in different cell types for its antiproliferative influence, there are only two publications addressing its effect on VSMC growth using angiotensin II (Ang II) and serum as stimuli, respectively (O'Sullivan et al., 2003; Li et al., 2008). Neither of these studies provides data regarding ROSC and PDGF signaling.

The study by Li et al. (2008) using Ang-II-activated VSMCs identifies ROSC as an inhibitor of ERK phosphorylation and activity, a mechanism that could be excluded in our setting. Reasons for this discrepancy could be next to the differing stimulus (Ang II versus PDGF), the pretreatment of cells for 15 h with ROSC before Ang II stimulation by Li et al., which may lead to secondary indirect effects due to changes in protein expression. However, even when pretreating our cells for 15 h or with up to 25 μM ROSC and 10 μM LGR1406, we were not able to detect changes in PDGF-mediated phosphorylation of ERK and other MAPK. Furthermore, cyclin D1

expression, a known target gene of ERK, is not inhibited by ROSC or LGR1406 (Ravenhall et al., 2000), again confirming that inhibition of cell cycle progression by ROSC and LGR1406 was not due to an interference with ERK signaling. It is noteworthy that cyclin D1 levels are even enhanced in response to ROSC and LGR1406 treatment, which may be due to a disturbed negative feedback loop between cell cycle progression and cyclin D1 expression.

The second study addressing ROSC and VSMCs used serum as a proliferative stimulus (O'Sullivan et al., 2003) and focused primarily on the differences in proliferation and the expression pattern of cell cycle regulators in human VSMCs from healthy media and in-stent-stenosis (ISS) sites. Because ISS-VSMCs expressed high levels of cyclins E and A, they used the CDK2 inhibitor ROSC. Consistent with our results, ROSC led to a delayed cell cycle progression, and it is noteworthy that ISS-VSMCs were more susceptible to ROSC treatment than those isolated from healthy vessels. These findings additionally highlight ROSC as an interesting lead for an antirestenotic therapy. Comparing ROSC and LGR1406, we clearly demonstrate that ROSC does not completely block PDGF-mediated VSMC cell cycle progression, whereas its novel derivative LGR1406 does. More precisely, the S-phase transition is blocked by LGR1406 but is only delayed by ROSC. Given the similar IC_{50} values in vitro and thus a comparable affinity of both compounds for CDK2, the kinase responsible for S-phase entry, the observed distinct effects of ROSC and LGR1406 might be due to either differences in their ability to permeate cells, their chemical or metabolic stability, or targets that might be affected by LGR1406 in addition to CDK2. Because ROSC is currently undergoing phase II clinical trials against breast cancer, there are multiple publications addressing its metabolism, pharmacokinetics, and stability issues (Raynaud et al., 2005; Vita et al., 2005a,b). ROSC is stable in human plasma up to 48 h at 0, 25, and 37°C and is insensitive to multiple freeze-thawing cycles (Vita et al., 2005a). Therefore, it is likely that chemical stability in cell culture medium is not responsible for the weaker activity of ROSC. Recently, a detailed study on ROSC metabolism in vitro and in vivo was published (McClue and Stuart, 2008). McClue and Stuart showed that ROSC is rapidly metabolized by rat liver microsomes, leading to a 50% reduction of parent compound after 90-min incubation. The major metabolite found was a carboxylate, which has been shown to have exceedingly higher IC_{50} values against

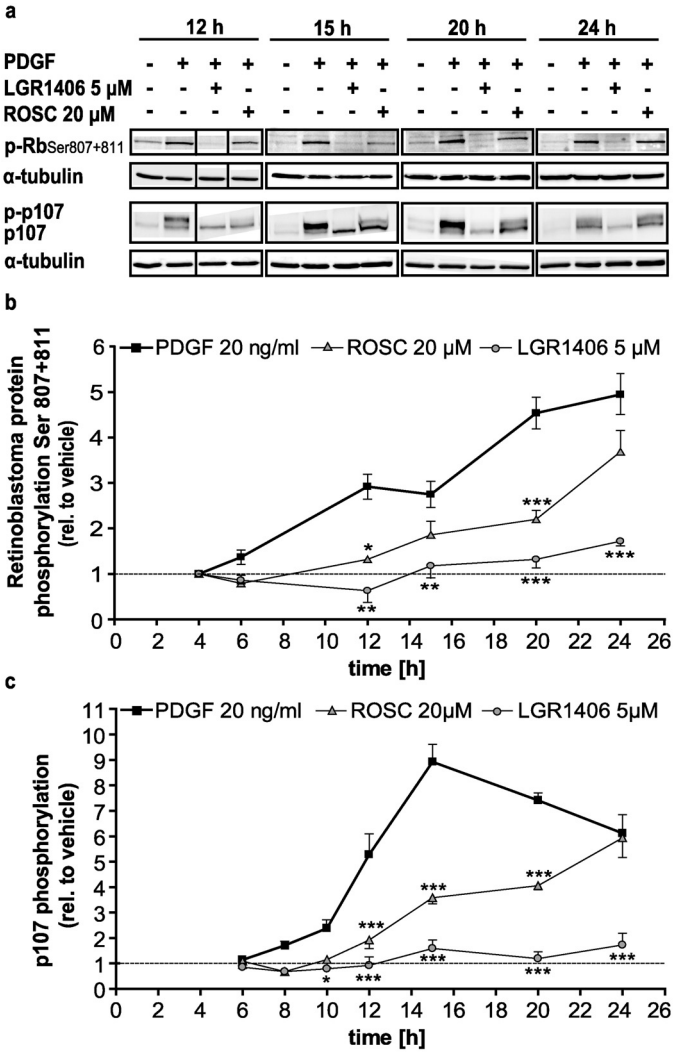

Fig. 5. Impact of LGR1406 and ROSC on pocket protein phosphorylation. Serum-starved VSMCs were pretreated for 30 min with LGR1406 (5 μM), ROSC (20 μM), or vehicle (DMSO 1%) before stimulation with PDGF-BB (20 ng/ml) for the indicated periods of time. Total cell lysates were then subjected to Western blot analysis of retinoblastoma protein phosphorylation ($pRb^{Ser807+811}$), p107/phospho-p107 (p-p107), and α-tubulin. a, representative Western blots out of at least three independent experiments with consistent results are shown for $pRb^{Ser807+811}$ and p-p107. b and c, graphs depict compiled data of the densitometrically evaluated phosphoprotein/tubulin ratios for each time point normalized to the respective unstimulated vehicle control. Shown are means ± S.E.M. *, $P < 0.05$, **, $P < 0.01$, ***, $P < 0.001$ (two-way ANOVA followed by Bonferroni post test versus PDGF treatment).

TABLE 1
IC_{50} values obtained from the in vitro kinase assay

	LGR1406	Roscovitine
	μM	
ALK	21	65
AMPK-α1[a]	33	>100
Aurora-A	0.6	>100
BRK	>100	>100
CDK1/CycB	3.2	9.9
CDK2/CycA	1.0	3.0
CDK2/CycE	0.6	0.5
CDK4/CycD1	15	29
CDK5/p25NCK	0.4	3.9
CDK6/CycD1	>100	27
CDK7/CycH/Mat1	>100	1.7
CDK9/CycT	1.1	1.6
EGFR	>100	>100
Focal adhesion kinase	13	51
FGF-R1	76	>100
FGF-R2	>100	>100
MEK1[b]	>100	>100
Nemo-like kinase	>100	99
p21-activated kinase 4	6.3	11
RAF-1[c]	>100	>100
Rho-associated, coiled-coil containing protein kinase 1	>100	>100
VEGF-R1	>100	>100
VEGF-R2	>100	>100
RSK1	9.1	N.D.
RSK3	N.D.	34

N.D., not determined; EGFR, epidermal growth factor receptor; FGF, fibroblast growth factor; MEK1, mitogen-activated protein kinase kinase 1; VEGF, vascular endothelial growth factor; RSK, ribosomal S6 kinase.
[a] LGR1406 was tested against a truncated version, roscovitine against the full-length AMPKα1.
[b] LGR1406 was tested against MEK SESE, roscovitine against wild-type MEK1.
[c] RAF1 Y340D/Y341D mutant was used.

CDK1/4 than ROSC itself but only slightly lower activity against CDK2 (Nutley et al., 2005). It is therefore conceivable that ROSC is differently or faster metabolized than LGR1406, carrying no hydroxyl group, in VSMC and thus exerts reduced or only transient activity toward its CDK targets. In silico calculations performed during this study supported the hypothesis of a more extensive metabolism of ROSC and predicted that 50% of ROSC is metabolized by CYP3A4 after 60 min of incubation with microsomal CYP3A4, which is in agreement with the published experimental data cited above (Nutley et al., 2005). In contrast, LGR1406 is suggested to be much more metabolically stable because only 25% of the compound is predicted to be metabolized after 60 min of incubation with microsomal CYP3A4.

The most striking difference between LGR1406 and ROSC with respect to the in vitro IC_{50} values obtained from the standardized ProQinase screening platform (Table 1) was that LGR1406 potently inhibits Aurora A kinase whereas ROSC does not. So far, Aurora A is reported to contribute to the regulation of M-phase entry. Depletion of Aurora A results in delayed entry into mitosis because it is able to phosphorylate Cdc25b, which in turn regulates the activation of the CDK1/cyclin B1 complex required for mitotic entry (Pollard and Mortimore, 2009). Increased expression and activity of Aurora A have so far been found exclusively in G_2 phase of the cell cycle. Because cells are blocked already in G_1 phase of the cell cycle in the presence of LGR1406, Aurora A seems an unlikely target in our setting. However, Aurora A is overexpressed in a variety of tumor types ranging from breast to prostate cancer, and corresponding inhibitors are already in preclinical studies (Gautschi et al., 2008; Zhou et al., 1998). Thus, further studies addressing a putative activity of LGR1406 against cancer cells with an increased Aurora A kinase activity are warranted. In summary, this study provides first evidence that optimized ROSC derivatives such as LGR1406 could serve as antiproliferative agents against VSMC proliferation that merit further evaluation as antirestenotic compounds.

References

Alessi F, Quarta S, Savio M, Riva F, Rossi L, Stivala LA, Scovassi AI, Meijer L, and Prosperi E (1998) The cyclin-dependent kinase inhibitors olomoucine and roscovitine arrest human fibroblasts in G1 phase by specific inhibition of CDK2 kinase activity. *Exp Cell Res* **245:**8–18.

Allen TR, Krueger KD, Hunter WJ 3rd, and Agrawal DK (2005) Evidence that insulin-like growth factor-1 requires protein kinase C-epsilon, PI3-kinase and mitogen-activated protein kinase pathways to protect human vascular smooth muscle cells from apoptosis. *Immunol Cell Biol* **83:**651–667.

Atanasova G, Jans R, Zhelev N, Mitev V, and Poumay Y (2005) Effects of the cyclin-dependent kinase inhibitor CYC202 (R-roscovitine) on the physiology of cultured human keratinocytes. *Biochem Pharmacol* **70:**824–836.

Bach S, Knockaert M, Reinhardt J, Lozach O, Schmitt S, Baratte B, Koken M, Coburn SP, Tang L, Jiang T, et al. (2005) Roscovitine targets, protein kinases and pyridoxal kinase. *J Biol Chem* **280:**31208–31219.

Benson C, White J, De Bono J, O'Donnell A, Raynaud F, Cruickshank C, McGrath H, Walton M, Workman P, Kaye S, et al. (2007) A phase I trial of the selective oral cyclin-dependent kinase inhibitor seliciclib (CYC202; R-Roscovitine), administered twice daily for 7 days every 21 days. *Br J Cancer* **96:**29–37.

Berellini G, Cruciani G, and Mannhold R (2005) Pharmacophore, drug metabolism, and pharmacokinetics models on non-peptide AT1, AT2, and AT1/AT2 angiotensin II receptor antagonists. *J Med Chem* **48:**4389–4399.

Bettayeb K, Oumata N, Echalier A, Ferandin Y, Endicott JA, Galons H, and Meijer L (2008) CR8, a potent and selective, roscovitine-derived inhibitor of cyclin-dependent kinases. *Oncogene* **27:**5797–5807.

Cianchetta G, Mannhold R, Cruciani G, Baroni M, and Cecchetti V (2004) Chemometric studies on the bactericidal activity of quinolones via an extended VolSurf approach. *J Med Chem* **47:**3193–3201.

Crivori P, Cruciani G, Carrupt PA, and Testa B (2000) Predicting blood-brain barrier permeation from three-dimensional molecular structure. *J Med Chem* **43:**2204–2216.

Crivori P, Zamora I, Speed B, Orrenius C, and Poggesi I (2004) Model based on GRID-derived descriptors for estimating CYP3A4 enzyme stability of potential drug candidates. *J Comput Aided Mol Des* **18:**155–166.

Cruciani G, Crivori P, Carrupt PA, and Testa B (2000) Molecular fields in quantitative structure-permeation relationships: the VolSurf approach. *Theochem* **503:**17–30.

Gautschi O, Heighway J, Mack PC, Purnell PR, Lara PN Jr, and Gandara DR (2008) Aurora kinases as anticancer drug targets. *Clin Cancer Res* **14:**1639–1648.

Heldin CH and Westermark B (1990) Platelet-derived growth factor: mechanism of action and possible in vivo function. *Cell Regul* **1:**555–566.

Krystof V, Moravcová D, Paprskárová M, Barbier P, Peyrot V, Hlobilková A, Havlícek L, and Strnad M (2006) Synthesis and biological activity of 8-azapurine and pyrazolo[4,3-d]pyrimidine analogues of myoseverin. *Eur J Med Chem* **41:**1405–1411.

Kukreja N, Onuma Y, Daemen J, and Serruys PW (2008) The future of drug-eluting stents. *Pharmacol Res* **57:**171–180.

Li AY, Han M, Zheng B, and Wen JK (2008) Roscovitine inhibits ERK1/2 activation induced by angiotensin II in vascular smooth muscle cells. *FEBS Lett* **582:**243–248.

Mannhold R, Cruciani G, Weber H, Lemoine H, Derix A, Weichel C, and Clementi M (1999) 6-Substituted benzopyrans as potassium channel activators: synthesis, vasodilator properties, and multivariate analysis. *J Med Chem* **42:**981–991.

McClue SJ and Stuart I (2008) Metabolism of the trisubstituted purine cyclin-dependent kinase inhibitor seliciclib (R-roscovitine) in vitro and in vivo. *Drug Metab Dispos* **36:**561–570.

Meijer L, Borgne A, Mulner O, Chong JP, Blow JJ, Inagaki N, Inagaki M, Delcros JG, and Moulinoux JP (1997) Biochemical and cellular effects of roscovitine, a potent and selective inhibitor of the cyclin-dependent kinases cdc2, cdk2 and cdk5. *Eur J Biochem* **243:**527–536.

Meijer L and Raymond E (2003) Roscovitine and other purines as kinase inhibitors. From starfish oocytes to clinical trials. *Acc Chem Res* **36:**417–425.

Mgbonyebi OP, Russo J, and Russo IH (1999) Roscovitine induces cell death and morphological changes indicative of apoptosis in MDA-MB-231 breast cancer cells. *Cancer Res* **59:**1903–1910.

Nutley BP, Raynaud FI, Wilson SC, Fischer PM, Hayes A, Goddard PM, McClue SJ, Jarman M, Lane DP, and Workman P (2005) Metabolism and pharmacokinetics of the cyclin-dependent kinase inhibitor R-roscovitine in the mouse. *Mol Cancer Ther* **4:**125–139.

O'Sullivan M, Scott SD, McCarthy N, Figg N, Shapiro LM, Kirkpatrick P, and Bennett MR (2003) Differential cyclin E expression in human in-stent stenosis smooth muscle cells identifies targets for selective anti-restenosis therapy. *Cardiovasc Res* **60:**673–683.

Oumata N, Bettayeb K, Ferandin Y, Demange L, Lopez-Giral A, Goddard ML, Myrianthopoulos V, Mikros E, Flajolet M, Greengard P, et al. (2008) Roscovitine-derived, dual-specificity inhibitors of cyclin-dependent kinases and casein kinases 1. *J Med Chem* **51:**5229–5242.

Pollard JR and Mortimore M (2009) Discovery and development of aurora kinase inhibitors as anticancer agents. *J Med Chem* **52:**2629–2651.

Ravenhall C, Guida E, Harris T, Koutsoubos V, and Stewart A (2000) The importance of ERK activity in the regulation of cyclin D1 levels and DNA synthesis in human cultured airway smooth muscle. *Br J Pharmacol* **131:**17–28.

Raynaud FI, Whittaker SR, Fischer PM, McClue S, Walton MI, Barrie SE, Garrett MD, Rogers P, Clarke SJ, Kelland LR, et al. (2005) In vitro and in vivo pharmacokinetic-pharmacodynamic relationships for the trisubstituted aminopurine cyclin-dependent kinase inhibitors olomoucine, bohemine and CYC202. *Clin Cancer Res* **11:**4875–4887.

Riccardi C and Nicoletti I (2006) Analysis of apoptosis by propidium iodide staining and flow cytometry. *Nat Protoc* **1:**1458–1461.

Steffel J, Eberli FR, Lüscher TF, and Tanner FC (2008) Drug-eluting stents - should be improved? *Ann Med* **40:**242–252.

Vita M, Abdel-Rehim M, Nilsson C, Hassan Z, Skansen P, Wan H, Meurling L, and Hassan M (2005a) Stability, pKa and plasma protein binding of roscovitine. *J Chromatogr B Analyt Technol Biomed Life Sci* **821:**75–80.

Vita M, Abdel-Rehim M, Olofsson S, Hassan Z, Meurling L, Sidén A, Sidén M, Pettersson T, and Hassan M (2005b) Tissue distribution, pharmacokinetics and identification of roscovitine metabolites in rat. *Eur J Pharm Sci* **25:**91–103.

Whittaker SR, Walton MI, Garrett MD, and Workman P (2004) The cyclin-dependent kinase inhibitor CYC202 (R-roscovitine) inhibits retinoblastoma protein phosphorylation, causes loss of Cyclin D1, and activates the mitogen-activated protein kinase pathway. *Cancer Res* **64:**262–272.

Windecker S and Jüni P (2008) Safety of drug-eluting stents. *Nat Clin Pract Cardiovasc Med* **5:**316–328.

Zhou H, Kuang J, Zhong L, Kuo WL, Gray JW, Sahin A, Brinkley BR, and Sen S (1998) Tumour amplified kinase STK15/BTAK induces centrosome amplification, aneuploidy and transformation. *Nat Genet* **20:**189–193.

Address correspondence to: Dr. Verena M. Dirsch, University of Vienna, Department of Pharmacognosy, Althanstr. 14, 1090 Vienna, Austria. E-mail: verena.dirsch@univie.ac.at